The pivotal role of von Willebrand factor binding to platelet αIIbβ3 in stabilizing the formation of a platelet plug at sites of injury

Qizhen Shi,[1-4] Jeremy G. Mattson,[1] Patricia A. Morateck,[1] Pamela A. Christopherson,[1] Jocelyn A. Schroeder,[1-4] Scot A. Fahs,[1] Jessica Rapten,[1] Marie L. Schulte,[1] Hartmut Weiler,[1,2] Jieqing Zhu,[1,2] Sandra L. Haberichter,[1,2] Veronica H. Flood[1-4] and Robert R. Montgomery[1,2]

[1]Thrombosis and Hemostasis Program, Versiti Blood Research Institute; [2]Departments of Pediatrics, Cell Biology, Neurology and Anatomic, and Biochemistry, Medical College of Wisconsin; [3]Children's Research Institute, Children's Wisconsin and [4]Midwest Athletes Against Childhood Cancer Fund Research Center, Milwaukee, WI, USA

Correspondence: Q. Shi
qshi@versiti.org

Received: February 26, 2025.
Accepted: May 9, 2025.
Early view: May 22, 2025.

https://doi.org/10.3324/haematol.2025.287685

Supplemental Data

Supplemental Methods

Antibodies and reagents

Agilent QuickChange II XL Mutagenesis kit was purchased from Agilent Technologies, Inc. (Santa Clara, CA). GoTaq Green Master Mix was purchased from Promega (Madison, WI). Alkaline Phosphatase-Streptavidin was purchased from Jackson ImmunoResearch Laboratories (West Grove, PA) and p-nitrophenyl phosphate (PNPP) substrate was from Life Technologies (Carlsbad, CA). Anti-mouse VWF monoclonal antibody (MoAb) 344.2, 332.2; anti-human VWF MoAb AVW1, 105.4, AVW4, and AVW15; anti-human GPIIIa (β_3) MoAb AP-3, and anti-mouse fibrin MoAb were produced by our hybridoma core laboratory. Rabbit anti-human VWF polyclonal antibody (PoAb), which also cross-reacts with mouse VWF, was purchased from Dako (Carpinteria, CA). Anti-mouse GPIIb MoAb (CD41) (clone MWReg30) was purchased from BD Biosciences (Franklin Lakes, NJ). Rat anti-GPIbβ monoclonal antibody conjugated with DyLight488 was purchased from Emfret Analytics (Eibelstadt, Germany). Alexa Fluor 647 was purchased from Invitrogen (ThermoFisher, MA). Both human and murine collagen-III and collagen-IV were purchased from Southern Biotech (Birmingham, AL). Human collagen-III and murine collagen-IV proteins were purchased from Southern Biotech (Birmingham, AL). Immulon 4HBX 96-well microplates were purchased from ThermoFisher (Rochester, NY). Ferric chloride was purchased from Sigma Aldrich (St. Louis, MO). Quinacrine dihydrochloride was purchased from Calbiochem/Millipore (Billerica, MA).

Patient populations and healthy controls

Eight hundred sixty-three subjects, including von Willebrand disease (VWD) index cases and their family members as well as healthy control (HC), enrolled from clinical hematology centers from 2005-2024 as part of the Zimmerman Program for Molecular and Clinical Biology of VWD[1] (see **Appendix**). Subjects with various types of VWD include type 1 [reduced amount of VWF produced], type-1C [increased VWF clearance], type 1S [type 1 severe, with trace measurable VWF:Ag], type-2A [deficiency of high molecular weight multimers], type-2B [increased binding of VWF-platelets through GPIb], type-2M [defect in the A1 domain of VWF gene which encodes for the GPIb receptor on the platelets or a missense mutation in the A3 domain, leading to reduced binding between platelets and VWF], type-2N [reduced binding affinity of VWF to FVIII]. Informed consent was obtained from all subjects, and the study was approved by the Institute Review Board (IRB). The bleeding scores were determined using the International Society of Thrombosis and Hemostasis Bleeding Assessment Tool (ISTH-BAT).[2] Full exonic Sanger-sequencing of the *VWF* gene identified variants in index cases and targeted sequencing confirmed these variants in family members. Central laboratory VWF testing was also conducted to validate phenotypic diagnoses as previously described.[3-6]

VWF-GPIIb/IIIa ($\alpha_{IIb}\beta_3$) binding activity assay

The biological function of VWF in binding to $\alpha_{IIb}\beta_3$ was quantified by our novel ELISA-based assay using an antibody-captured recombinant $\alpha_{IIb}\beta_3$ headpiece protein,[7-9] as depicted in **Figure 1A**. For the human VWF:$\alpha_{IIb}\beta_3$ binding assay, a 96-well Immulon 4HBX plate was coated with 50 µl/well of anti-human GPIIIa (β_3 integrin) MoAb AP-3 at a concentration of 5 µg/ml at 4°C overnight. After being washed with TBST buffer (20 mM Tris-HCl, 150 mM NaCl, 1mM $CaCl_2$, 1 mM $MgCl_2$, 1 mM $MnCl_2$, 0.1% Tween-20, pH7.5) twice and blocked with TBS block buffer

(20 mM Tris-HCl, 150mM NaCl, 1mM $CaCl_2$, 1 mM $MgCl_2$, 1 mM $MnCl_2$, 1% BSA) at room temperature for 1 hour, 50 µl of 0.25 µg/ml recombinant human $\alpha_{IIb}\beta_3$ headpiece[7-9] was added and incubated at room temperature for 1 hour. Plasma samples were defibrinated by incubating at 56°C for 15 minutes, followed by centrifugation at 12000g for 10 minutes. Fifty microliters of diluted heat-defibrinated plasma (HDP) samples (1:50) were added to each well in duplicates and incubated at room temperature for 1 hour. After being washed three times, 50 µl/well of 1 µg/ml biotinylated AVW15 anti-human VWF MoAb was added and incubated at room temperature for 30 minutes. After being washed, 50 µl/well of 1:5000 streptavidin-alkaline phosphatase was added and incubated at room temperature for 30 minutes. After being washed, 100 µl/well of PNPP (p-nitrophenyl phosphate) substrate was added to the plate, and optical density was read at 405-650 nm using a SpectraMax Plus 384 Microplate Reader (Molecular Devices, San Jose, CA). Pooled human plasma from the Scientific and Standardization Committee (SSC) and International Society of Thrombosis and Hemostasis (ISTH) lot#5 was defibrinated and used as the standard. For determining mouse VWF:$\alpha_{IIb}\beta_3$ binding activity, two protocols were developed. One was to measure mouse VWF binding capacity to human $\alpha_{IIb}\beta_3$ [mVWF:h$\alpha_{IIb}\beta_3$] using recombinant human $\alpha_{IIb}\beta_3$ headpiece, and the other was to mouse $\alpha_{IIb}\beta_3$ [mVWF:m$\alpha_{IIb}\beta_3$] using recombinant mouse $\alpha_{IIb}\beta_3$ (m$\alpha_{IIb}\beta_3$) headpiece purified from stably transfected HEK293F cells. The biotinylated Dako rabbit anti-human VWF PoAb was used to detect bound VWF, and a defibrinated plasma pool from C57BL/6J mice was used as the standard for mVWF:h$\alpha_{IIb}\beta_3$ assay and pooled plasma from $Fib^{-/-}$ mice without defibrinated was used as the standard for mVWF:m$\alpha_{IIb}\beta_3$ assay. The sensitivity of this assay was 1 mU/ml (0.01 U/dl).

Mice

All mice used in this study were in the C57BL/6J background. Wild-type (WT) C57BL/6J mice and VWF knockout ($VWF^{-/-}$) mice[10] were purchased from the Jackson Laboratory and back-crossed in-house. Fibrinogen knockout ($Fib^{-/-}$)[11] and γΔ5 variant (($Fib^{\Delta5/\Delta5}$)[12] were kind gifts from Dr. Mathew Flick at the University of North Carolina at Chapel Hill. All mice were maintained in pathogen-free micro-isolator cages at animal facilities operated by the Medical College of Wisconsin. All animal studies were performed according to protocols approved by the Institutional Animal Care and Use Committee of the Medical College of Wisconsin. Isoflurane or ketamine was used for anesthesia.

Generation of VWD with RGES variant mouse models

The change of *VWF* c.7527T>A (p.Asp2509Glu), which converts the RGDS motif to RGeS [termed RGES] impairing VWF binding to activated platelets as previously reported in an *in vitro* study,[13] was introduced into cloned mouse *VWF* cDNA by Quick-Change mutagenesis using the Agilent QuickChange II XL Mutagenesis kit, and the variant was confirmed to cause a severe $\alpha_{IIb}\beta_3$-binding defect when expressed *in vitro* in HEK293T cells.

A CRISPR-Cas9 strategy was used to generate a VWF-RGES variant mouse model. A guide RNA (gRNA) targeting exon-44 of the mouse *VWF* gene was cloned into a plasmid that expresses both the gRNA and Cas9. As shown in **Figure 3A**, an asymmetric single-stranded oligodeoxynucleotide (ssODN) homology-directed repair (HDR) template spanning the predicted Cas9 cleavage site was designed to introduce three single nucleotide changes into the *VWF* gene following procedures as reported.[14,15] In addition to the c.7527T>A RGeS mutation, two silent

mutations were included; c.7518G>C and c.7521G>C, creating a new diagnostic SacII (cGGcG/G) at cDNA base 7522.

The gRNA/Cas9 plasmid and HDR template were mixed and injected into C57BL/6J mouse zygotes. The resulting founders were bred with C57BL/6J mice to establish 4 independent type VWF-RGES lineages. The introduced c.7527T>A variant was confirmed by sequencing. Heterozygous $VWF^{RGES/+}$ offspring were crossed to generate the homozygous $VWF^{RGESRGES}$ model and additional $VWF^{RGES/+}$ and wild-type (WT) $VWF^{+/+}$ controls. $VWF^{RGES/RGES}$ mice were crossed with fibrinogen deficient ($Fib^{-/-}$)[11] or γ-chain variant ($Fib^{\gamma\Delta5/\gamma\Delta5}$), which abolishes the fibrinogen binding motif but expression is normal,[12] mice to generate $Fib^{-/-}VWF^{RGES/RGES}$ and $Fib^{\gamma\Delta5/\gamma\Delta5}VWF^{RGES/RGES}$ mice. The VWF-RGES genotype was confirmed by PCR of DNA purified from peripheral blood leukocytes using GoTaq Green Master Mix with primers 5'-TTATCCATCCCCTCCCCAGG-3' (forward) and 5'-TAGACCTGCGAAACCAGCTG-3' (reverse) flanking exon 44. The PCR product was digested with restriction enzyme SacII and ran on 1.25% agarose gel electrophoresis to distinguish wild-type and mutated alleles. Distilled water was used as a negative control in parallel for PCR. $Fib^{-/-}$ and $Fib^{\Delta5/\Delta5}$genotypes were determined by PCR as previously reported.[11,12]

VWF antigen (VWF:Ag) and VWF-collagen binding (VWF:CB) activity assays

Blood samples were collected by tail bleed, and plasma was isolated as described previously by our laboratory.[16] VWF antigen (VWF:Ag) levels in mouse plasma were determined by enzyme-linked immunosorbent assay (ELISA) following the protocol as previously described.[15,17] Briefly, anti-mouse VWF MoAb 344.2 coated 96-well plates were used to capture mouse

VWF:Ag from diluted plasma. Bound VWF was detected with biotin-conjugated MoAb 332.2, Alkaline Phosphatase-Streptavidin, and p-nitrophenyl phosphate (PNPP). Optical density was read at 405 nm using a Microplate Reader. Pooled plasma from C57BL/6J mice was used as the standard. For human VWF:Ag ELISA, mouse anti-human VWF MoAb AVW1 and 105.4 capture antibodies and biotinylated AVW4 and AVW15 detection antibodies were used. Pooled plasma from healthy human individuals (SSC/ISTH Lot#5) was used as the standard.

To determine the biological functions of RGES-VWF in binding to collagen, we performed binding assays for VWF/collagen-III (VWF:CB3) and VWF/collagen-IV (VWF:CB4) using samples collected from patients with VWD and healthy subjects as well as $VWF^{RGES/RGES}$ mice and their littermate $VWF^{RGES/+}$ and $VWF^{+/+}$ mice and analyzed following procedures as previously described.[18-20] Pooled human healthy individual plasma from SSC/ISTH and WT C57BL/6J mice were used as a standard for human-VWF:CB and mouse-VWF:CB studies, respectively.

Phenotypic assessments

The bleeding phenotype in RGES-VWF mice was assessed by three *in vitro* assays: rotational thromboelastometry (ROTEM) assay, nWB-TGA, and Venaflux, following procedures described in our previous reports,[18,21,22] and by five *in vivo* vessel injury models: 1) lateral tail vein transection (TVT) injury;[15,23-25] 2) tail tip transection (TTT) by clipping 4-mm of the tail tip by length for a 20 min bleeding test,[15] 3) 6-hour tail bleeding test,[26-32] 4) $FeCl_3$-induced carotid artery injury,[33] and 5) cremaster intravital laser injury.[34,35]

For the TVT, TTT, 6-hour tail bleeding tests, and $FeCl_3$-induced carotid artery injury, we used protocols following procedures as described in our previous reports.[15,26,33] Briefly, for the TVT model, the injury in the left lateral tail vein was induced using a scalpel blade with a template cutting block to cut at a diameter of 2.5 mm of the tail from animals under isoflurane anesthesia. The wounded tail was placed into 14 ml of pre-warmed saline, and animals were monitored for 15 minutes as the primary bleeding time and rechallenged 3 times if the bleeding stopped or at 15 minutes if it did not stop. Blood loss from the primary and rechallenged injuries was collected, and hemoglobin levels were measured at a wavelength of 575 nm after lysing red blood cells in dH_2O against a standard generated from a known amount of pooled whole blood from C57BL/6J mice. For the TTT, a 4 mm length tail tip was severed from isoflurane-anesthetized mice using a scalpel. The wounded tail was placed into 14 ml of pre-warmed saline, and animals were monitored for 20 minutes without rechallenge. The bleeding time was recorded, and blood loss was quantified as described above. Both TVT and TTT assays were blinded. For the 6-hour tail bleeding test, the tail tip from anesthetized animals was severed by scalpel using a 1.6 mm diameter template. Animals were monitored hourly for 6 hours and tail bleeding time was recorded. Fifty microliters of blood were collected before and after the test, and hemoglobin levels were measured using Animal Blood Counter.

For the $FeCl_3$-induced carotid artery injury test, we followed the procedures described in our previous report.[33] Briefly, the right carotid artery of anesthetized mice was exposed, and a 1x2 mm filter paper soaked in 15% ferric chloride was applied for 3 minutes. Following removal, the artery was washed three times with warm PBS to clear any residual ferric chloride. A Doppler ultrasound flow probe (Model MA0.5PSB, Transonic Systems, Ithaca, NY) was placed on the

artery to monitor blood flow. The time to occlusion (TTO) was defined as the duration from filter paper removal until blood flow ceased for three consecutive minutes, with a maximum observation time of 45 minutes.

For cremaster intravital laser injury, the experiments were performed in collaboration with Versiti Blood Research Institute Imaging Core, following the procedures as previously reported.[34,35] Briefly, intravital imaging of platelet thrombus formation in mouse cremaster arterioles was performed in the Thrombosis Core of the Versiti Blood Research Institute. Male mice were anesthetized with ketamine/dexmedetomidine and the body temperature was maintained at 37°C using a thermoregulated heating pad. The cremaster muscle was exposed, spread out, and superfused with warmed saline (37°C) suffused with 5% CO_2 in N_2 balance. Alexa Fluor 647-labeled anti-fibrin antibody 59D8 (0.5 mg/kg; Hybridoma Core Laboratory, Versiti Blood Research Institute, Milwaukee) and DyLight 488-labeled anti-platelet GPIbβ (0.1 mg/kg; Emfret Analytics) were injected retro-orbitally. At least 20 min after injection, arteriolar wall injury was induced with a laser ablation system (Intelligent Imaging Innovations) using an enclosed pulsed laser (532 nm; >5 pules). Laser intensity and duration were adjusted to produce an injury visible in the brightfield image. Fluorescence images were captured using a high-speed camera (Orca Flash4.0, Hamamatsu). Data were collected for at least 2 min following vessel injury. The arteriolar thrombus formation and embolization were monitored and captured. The fluorescence intensity of accumulated platelets and fibrin in thrombi and emboli was expressed in relative fluorescence units (RFU). In addition to the standard thrombus measurement, we assessed embolic events downstream of the thrombus. To do this, we created an embolism mask region spanning the vessel's full diameter. This region was placed so that it was not impacted by

the growing thrombus. Emboli in this region were assessed by labeled platelet aggregates passing through this region above the in-vessel background. Emboli were then quantified over time as an area under the curve of the fluorescent signal.

Statistical analysis

Data are presented as the mean ± SD. Statistical comparisons of two experimental groups were evaluated using the unpaired Student's *t*-test or Mann-Whitney *U*-test. The one-way ANOVA followed by Fisher's Least Significant Difference (LSD) test was used to determine whether there were statistically significant differences among the means of three or more groups. The two-way ANOVA followed by Fisher's LSD test was used for multiple comparisons between groups in the primary and re-challenge bleeding tests. The simple linear regression was employed to evaluate the correlation between two data sets. Statistical analysis was performed using GraphPad Prism 10 (GraphPad Software, La Jolla, CA) and SigmaPlot 14.0 (Systat Software, Inc. San Jose, CA). A value of $P < 0.05$ was considered statistically significant.

Legend for Supplemental Videos

To assess the bleeding and embolism phenotype in VWF^{RGES} mice, we performed intravital laser injury on cremaster arterioles to investigate how RGES-VWF affects clot stability.

Male mice were anesthetized with a mixture of ketamine (75 mg/kg) and dexmedetomidine (0.5 mg/kg). The arterioles in the cremaster muscle were exposed. Fluorophore-labeled antibodies were injected retro-orbitally to label fibrin and platelets. Fibrin was labeled with an anti-fibrin monoclonal antibody conjugated to Alexa Fluor 647, while platelets were labeled with a rat anti-mouse GPIbβ monoclonal antibody conjugated to DyLight 488. The vascular injury was induced

using an enclosed pulsed laser, and the arteriolar thrombus formation and embolization were monitored and captured. Representative recorded videos from the intravital laser injury model of VWF-RGES and wild-type C57BL/6 mice were presented in the Supplemental Videos. (A). Cremaster arteriole Laser injury model_C57BL6-WT. (B). Cremaster arteriole laser injury model_VWF-RGES.

Reference List

1. Montgomery RR, Flood VH. What have we learned from large population studies of von Willebrand disease? Hematology Am Soc Hematol Educ Program 2016;2016(1):670-677. DOI: 10.1182/asheducation-2016.1.670.
2. Rodeghiero F, Tosetto A, Abshire T, et al. ISTH/SSC bleeding assessment tool: a standardized questionnaire and a proposal for a new bleeding score for inherited bleeding disorders. J Thromb Haemost 2010;8(9):2063-5. DOI: 10.1111/j.1538-7836.2010.03975.x.
3. Christopherson PA, Tijet N, Haberichter SL, et al. The common VWF variant p.Y1584C: detailed pathogenic examination of an enigmatic sequence change. J Thromb Haemost 2024;22(3):666-675. DOI: 10.1016/j.jtha.2023.11.016.
4. Roberts JC, Christopherson PA, Tarantino MD, et al. Von Willebrand Factor (VWF) multiplex activity assay differentiation of type 1 von Willebrand Disease (VWD) and variant VWD. Haemophilia 2024;30(1):161-168. DOI: 10.1111/hae.14901.
5. Sadler B, Christopherson PA, Perry CL, et al. Characterization of copy-number variants in a large cohort of patients with von Willebrand disease reveals a relationship between disrupted regions and disease type. Res Pract Thromb Haemost 2023;7(7):102232. DOI: 10.1016/j.rpth.2023.102232.
6. Sadler B, Christopherson PA, Haller G, Montgomery RR, Di Paola J. von Willebrand factor antigen levels are associated with burden of rare nonsynonymous variants in the VWF gene. Blood 2021;137(23):3277-3283. DOI: 10.1182/blood.2020009999.
7. Zhu J, Zhu J, Negri A, et al. Closed headpiece of integrin alphaIIbbeta3 and its complex with an alphaIIbbeta3-specific antagonist that does not induce opening. Blood 2010;116(23):5050-9. DOI: 10.1182/blood-2010-04-281154.
8. Zhu J, Choi WS, McCoy JG, et al. Structure-guided design of a high-affinity platelet integrin alphaIIbbeta3 receptor antagonist that disrupts Mg(2)(+) binding to the MIDAS. Sci Transl Med 2012;4(125):125ra32. DOI: 10.1126/scitranslmed.3003576.
9. Zhu J, Zhu J, Springer TA. Complete integrin headpiece opening in eight steps. J Cell Biol 2013;201(7):1053-68. DOI: 10.1083/jcb.201212037.
10. Denis C, Methia N, Frenette PS, et al. A mouse model of severe von Willebrand disease: defects in hemostasis and thrombosis. Proc Natl Acad Sci U S A 1998;95(16):9524-9529. (http://www.ncbi.nlm.nih.gov/pubmed/9689113).
11. Suh TT, Holmback K, Jensen NJ, et al. Resolution of spontaneous bleeding events but failure of pregnancy in fibrinogen-deficient mice. Genes Dev 1995;9(16):2020-2033. DOI: 10.1101/gad.9.16.2020 [doi].

12. Holmback K, Danton MJ, Suh TT, Daugherty CC, Degen JL. Impaired platelet aggregation and sustained bleeding in mice lacking the fibrinogen motif bound by integrin alpha IIb beta 3. EMBO J 1996;15(21):5760-5771. (http://www.ncbi.nlm.nih.gov/pubmed/8918453).
13. Beacham DA, Wise RJ, Turci SM, Handin RI. Selective inactivation of the Arg-Gly-Asp-Ser (RGDS) binding site in von Willebrand factor by site-directed mutagenesis. J Biol Chem 1992;267(5):3409-15. (https://www.ncbi.nlm.nih.gov/pubmed/1737795).
14. Richardson CD, Ray GJ, DeWitt MA, Curie GL, Corn JE. Enhancing homology-directed genome editing by catalytically active and inactive CRISPR-Cas9 using asymmetric donor DNA. Nat Biotechnol 2016;34(3):339-344. DOI: nbt.3481 [pii];10.1038/nbt.3481 [doi].
15. Shi Q, Fahs SA, Mattson JG, et al. A novel mouse model of type 2N VWD was developed by CRISPR/Cas9 gene editing and recapitulates human type 2N VWD. Blood Adv 2022;6(9):2778-2790. DOI: 483434 [pii];10.1182/bloodadvances.2021006353 [doi].
16. Shi Q, Fahs SA, Kuether EL, Cooley BC, Weiler H, Montgomery RR. Targeting FVIII expression to endothelial cells regenerates a releasable pool of FVIII and restores hemostasis in a mouse model of hemophilia A. Blood 2010;116(16):3049-3057. DOI: blood-2010-03-272419 [pii];10.1182/blood-2010-03-272419 [doi].
17. Shi Q, Schroeder JA, Kuether EL, Montgomery RR. The important role of von Willebrand factor in platelet-derived FVIII gene therapy for murine hemophilia A in the presence of inhibitory antibodies. J Thromb Haemost 2015;13(7):1301-1309. DOI: 10.1111/jth.13001 [doi].
18. Flood VH, Schlauderaff AC, Haberichter SL, et al. Crucial role for the VWF A1 domain in binding to type IV collagen. Blood 2015. DOI: blood-2014-11-610824 [pii];10.1182/blood-2014-11-610824 [doi].
19. Flood VH, Gill JC, Christopherson PA, et al. Comparison of type I, type III and type VI collagen binding assays in diagnosis of von Willebrand disease. J Thromb Haemost 2012;10(7):1425-32. DOI: 10.1111/j.1538-7836.2012.04747.x.
20. Slobodianuk TL, Kochelek C, Foeckler J, Kalloway S, Weiler H, Flood VH. Defective collagen binding and increased bleeding in a murine model of von Willebrand disease affecting collagen IV binding. J Thromb Haemost 2019;17(1):63-71. DOI: 10.1111/jth.14341.
21. Zhang G, Shi Q, Fahs SA, Kuether EL, Walsh CE, Montgomery RR. Factor IX ectopically expressed in platelets can be stored in alpha-granules and corrects the phenotype of hemophilia B mice. Blood 2010;116(8):1235-1243. DOI: blood-2009-11-255612 [pii];10.1182/blood-2009-11-255612 [doi].
22. Baumgartner CK, Zhang G, Kuether EL, Weiler H, Shi Q, Montgomery RR. Comparison of platelet-derived and plasma factor VIII efficacy using a novel native whole blood thrombin generation assay. J Thromb Haemost 2015;13(12):2210-2219. DOI: 10.1111/jth.13169 [doi].
23. Johansen PB, Tranholm M, Haaning J, Knudsen T. Development of a tail vein transection bleeding model in fully anaesthetized haemophilia A mice - characterization of two novel FVIII molecules. Haemophilia 2016;22(4):625-631. DOI: 10.1111/hae.12907 [doi].
24. Garcia J, Flood VH, Haberichter SL, et al. A rat model of severe VWD by elimination of the VWF gene using CRISPR/Cas9. Res Pract Thromb Haemost 2020;4(1):64-71. DOI: 10.1002/rth2.12280 [doi];RTH212280 [pii].

25. Swystun LL, Georgescu I, Mewburn J, et al. Abnormal von Willebrand factor secretion, factor VIII stabilization and thrombus dynamics in type 2N von Willebrand disease mice. J Thromb Haemost 2017;15(8):1607-1619. DOI: 10.1111/jth.13749 [doi].
26. Chen Y, Schroeder JA, Kuether EL, Zhang G, Shi Q. Platelet gene therapy by lentiviral gene delivery to hematopoietic stem cells restores hemostasis and induces humoral immune tolerance in FIX(null) mice. Mol Ther 2014;22(1):169-177. DOI: mt2013197 [pii];10.1038/mt.2013.197 [doi].
27. Schroeder JA, Chen Y, Fang J, Wilcox DA, Shi Q. In vivo enrichment of genetically manipulated platelets corrects the murine hemophilic phenotype and induces immune tolerance even using a low multiplicity of infection. J Thromb Haemost 2014;12(8):1283-1293. DOI: 10.1111/jth.12633 [doi].
28. Chen Y, Luo X, Schroeder JA, et al. Immune tolerance induced by platelet-targeted factor VIII gene therapy in hemophilia A mice is CD4 T cell mediated. J Thromb Haemost 2017;15(10):1994-2004. DOI: 10.1111/jth.13800 [doi].
29. Gao C, Schroeder JA, Xue F, et al. Nongenotoxic antibody-drug conjugate conditioning enables safe and effective platelet gene therapy of hemophilia A mice. Blood Adv 2019;3(18):2700-2711. DOI: bloodadvances.2019000516 [pii];10.1182/bloodadvances.2019000516 [doi].
30. Chen J, Schroeder JA, Luo X, Montgomery RR, Shi Q. The impact of GPIbalpha on platelet-targeted FVIII gene therapy in hemophilia A mice with pre-existing anti-FVIII immunity. J Thromb Haemost 2019;17(3):449-459. DOI: 10.1111/jth.14379 [doi].
31. Schroeder JA, Chen J, Chen Y, et al. Platelet-targeted hyperfunctional FIX gene therapy for hemophilia B mice even with preexisting anti-FIX immunity. Blood Adv 2021;5(5):1224-1238. DOI: 475339 [pii];10.1182/bloodadvances.2020004071 [doi].
32. Jing W, Baumgartner CK, Xue F, Schroeder JA, Shi Q. Pre-existing anti-factor VIII immunity alters therapeutic platelet-targeted factor VIII engraftment following busulfan conditioning through cytotoxic CD8 T cells. J Thromb Haemost 2023;21(3):488-498. DOI: S1538-7836(22)07175-6 [pii];10.1016/j.jtha.2022.10.006 [doi].
33. Baumgartner CK, Mattson JG, Weiler H, Shi Q, Montgomery RR. Targeting factor VIII expression to platelets for hemophilia A gene therapy does not induce an apparent thrombotic risk in mice. J Thromb Haemost 2017;15(1):98-109. DOI: 10.1111/jth.13436 [doi].
34. Kim KH, Barazia A, Cho J. Real-time imaging of heterotypic platelet-neutrophil interactions on the activated endothelium during vascular inflammation and thrombus Formation in live mice. J Vis Exp 2013(74). DOI: 10.3791/50329.
35. Neyman M, Gewirtz J, Poncz M. Analysis of the spatial and temporal characteristics of platelet-delivered factor VIII-based clots. Blood 2008;112(4):1101-1108. DOI: blood-2008-04-152959 [pii];10.1182/blood-2008-04-152959 [doi].

Supplemental Figure 1

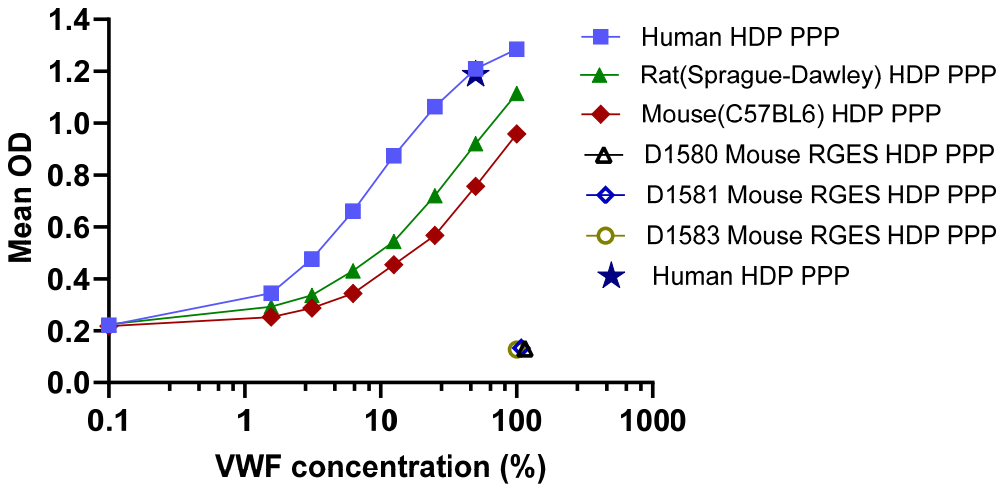

Supplemental Figure 1. Assessment of the viability of our assay on the binding of VWF in heat-defibrinated plasma (HDP) samples from humans, rats, and mice to immobilized recombinant human $\alpha_{IIb}\beta_3$ integrin (VWF:$\alpha_{IIb}\beta_3$). For the functional VWF:$\alpha_{IIb}\beta_3$ binding assay, an anti-human GPIIIa (β_3) monoclonal antibody (AP-3) was coated on a 96-well plate, and recombinant human $\alpha_{IIb}\beta_3$ headpiece was captured from a 0.25 μg/ml solution. Pooled platelet-poor plasma (PPP) from normal humans, rats, and mice, as well as plasma from three VWF-RGES homozygous mice (D1580, D1581, and D1583), were heated and defibrinated. Serial diluted HDP samples from normal pools, along with HDP plasma from VWF^{RGES} mice, were incubated with the antibody captured $\alpha_{IIb}\beta_3$. Unbound VWF was washed off, and the remaining $\alpha_{IIb}\beta_3$-bound VWF was detected. For human samples, biotinylated mouse anti-human VWF AVW15 monoclonal antibody was used for detection. For rat and mouse samples, biotinylated rabbit anti-human VWF polyclonal antibody (Dako), known to cross-react with mouse and rat VWF, was used for the detection. These results demonstrate that our novel functional VWF:$\alpha_{IIb}\beta_3$ binding activity assay is sensitive and reliable for human and rodent HDP samples.

Supplemental Figure 2

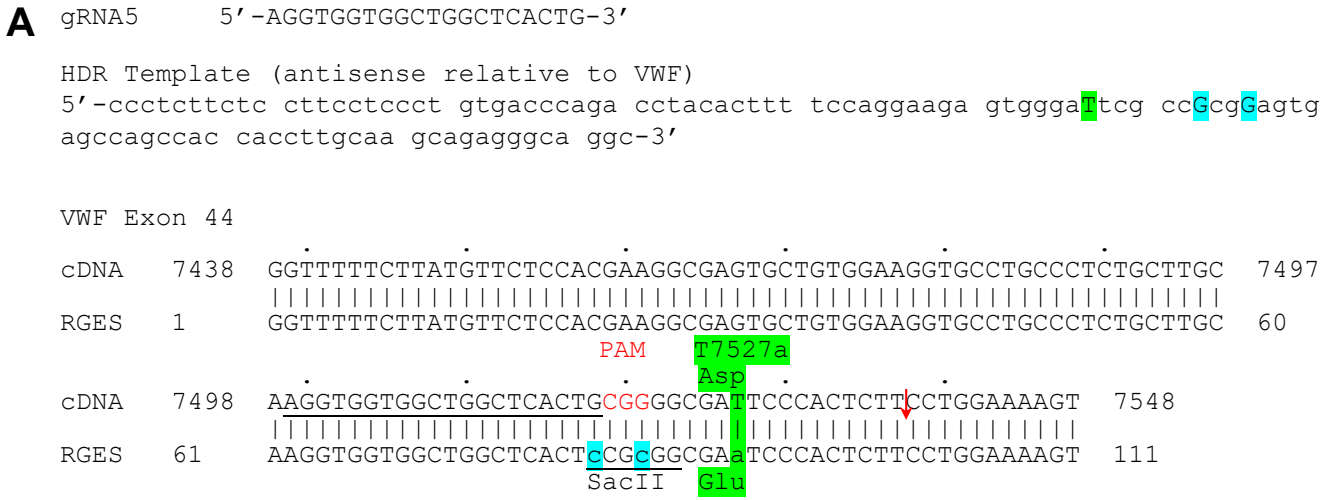

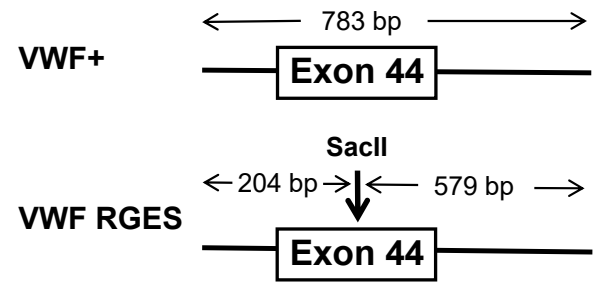

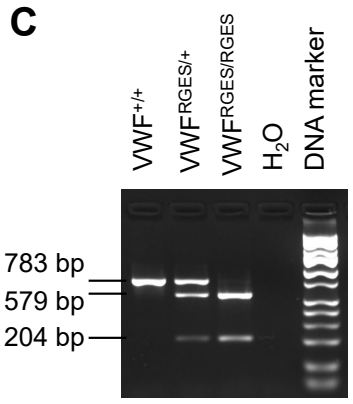

Supplemental Figure 2. Establishing the RGES variant VWD (VWF^{RGES}) mouse model using a CRISPR/Cas9 strategy. (**A**) A guide RNA (gRNA) and an asymmetric single-stranded oligodeoxynucleotide (ssODN) homology-directed repair template were designed to introduce three nucleotide changes into the mouse *VWF* gene near the predicted Cas9 cleavage site. The c.7527T>A *VWF* mutation converts the RGDS sequence to the RGES variant found in von Willebrand disease (VWD). The other two changes are silent mutations: c.7519G>C and c.7521G>C. These modifications eliminate the protospacer adjacent motif (PAM) sequence required by Cas9 and create a diagnostic Sac II site for genotyping, respectively. (**B**) The schematic diagram illustrates the genotyping process through PCR and subsequent digestion with the Sac II restriction enzyme. (**C**) PCR genotyping. DNA was purified from peripheral blood leukocytes, and a 783 bp fragment of the mouse *VWF* gene was amplified. The PCR product was then digested with SacII and run on a 2% agarose gel. For the wild-type mouse *Vwf* PCR product, a single uncut fragment of 783 bp was observed, as it does not contain a Sac II restriction enzyme site. In contrast, the mutated RGES mouse *VWF* gene produced two fragments, 579 bp and 204 bp, after digestion with Sac II. Thus, the VWF$^{+/+}$ genotype is indicated by a single 783 bp band, the VWF$^{RGES/RGES}$ genotype is characterized by the presence of 579 bp and 204 bp bands, and the VWF$^{RGES/+}$ genotype presents with all three bands: 783 bp, 579 bp, and 204 bp. H_2O was used as a negative control.

Supplemental Figure 3

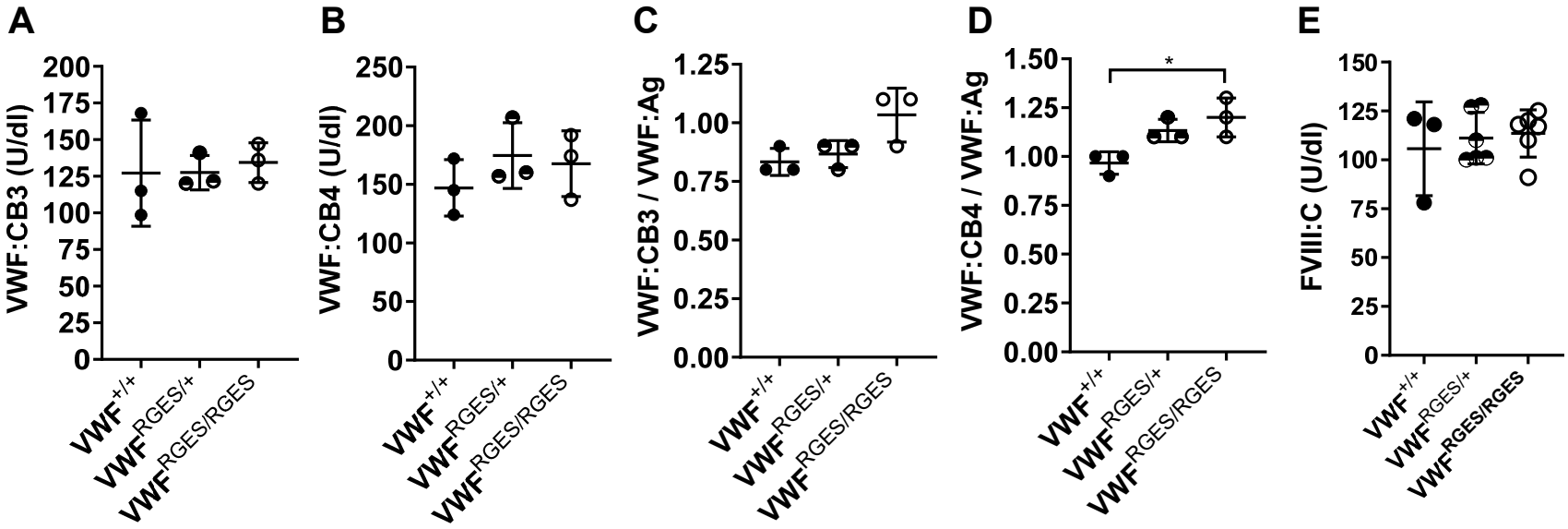

Supplemental Figure 3. Assessment of the functional VWF binding activity to collagen III and IV (VWF:CB3 and VWF:CB4) as well as plasma FVIII levels in VWF-RGES mice. Plasma samples were collected from mice through tail bleeds for the assays. For VWF:CB binding assay, collagen III or IV was coated on a 96-well plate at 1 μg/ml, and plasma samples were added to the collagen-coated plate and incubated. Unbound VWF was washed off, and the remaining collagen-bound VWF was detected using a biotinylated rabbit anti-human VWF polyclonal antibody (Dako), which is known to cross-react with mouse VWF. Mouse VWF antigen (mVWF:Ag) levels were determined by ELISA assay using anti-mouse VWF monoclonal antibody 344.2 for capture and biotinylated anti-VWF Dako antibody for detection. To quantify FVIII activity levels in the plasmas, we used a chromogenic assay. Plasma pooled from our wild-type C57BL/6J colony after heated defibrination was used as the standard. The plasma from wild-type VWF ($VWF^{+/+}$) and heterozygous $VWF^{+/-}$ littermates served as parallel controls. (**A**) VWF:CB3 levels. (**B**) VWF:CB4 levels. (**C**) The ratio of VWF:CB3/VWF:Ag. (**D**) The ratio of VWF:CB4/VWF:Ag. (**E**) FVIII activity levels. *$P < .05$. These results demonstrate that the VWF-RGES variant does not impair the VWF binding to collagen and FVIII expression in mice.

Supplemental Figure 4

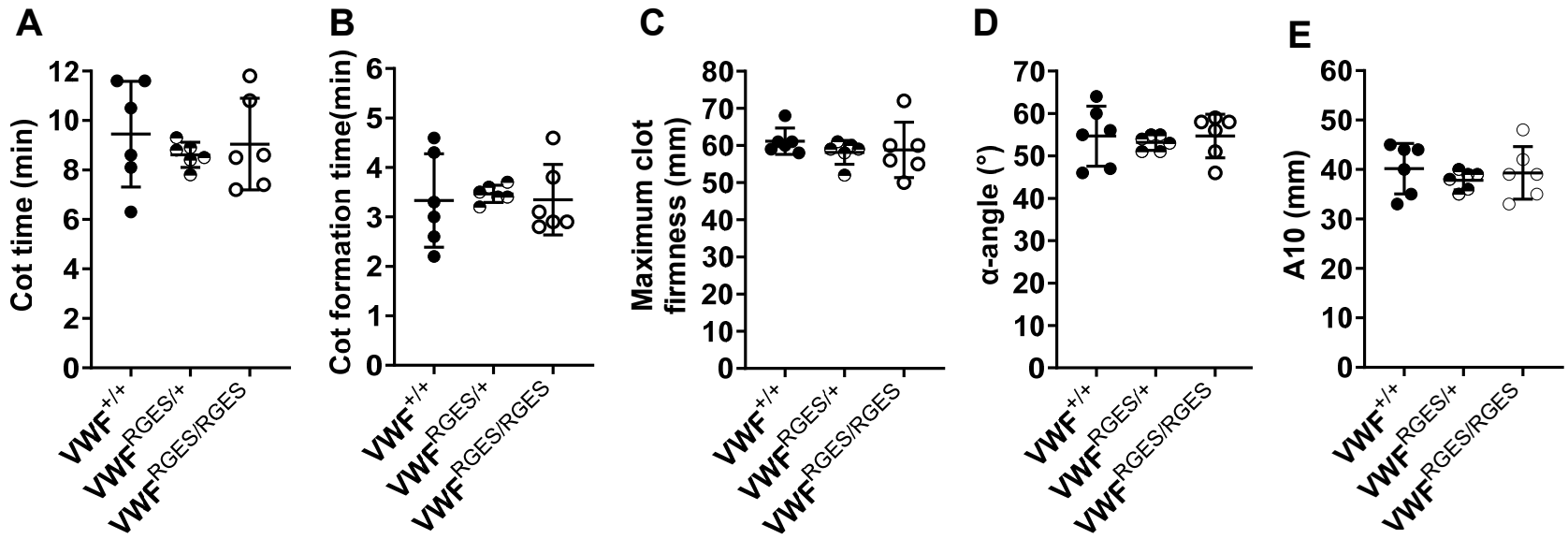

Supplemental Figure 4. Assessment of the biological hemostatic properties in VWF-RGES mice whole blood by ROTEM analysis. Blood samples were collected from the vena cava (terminal experiment) using 3.8% sodium citrate as an anticoagulant (vol/vol 1:10) and analyzed by native non-activated ROTEM analysis. ROTEM standard cups were preloaded with 21 µl of 0.2M $CaCl_2$, then 300 µl of whole blood was added, and clot formation was recorded using the NATEM measurement until maximum clot firmness reached its peak. $VWF^{+/+}$ and $VWF^{RGES/+}$ littermates served as controls. (**A**) Clot time. (**B**) Clot formation time. (**C**) Maximum clot firmness. (**D**) α-angle. (**E**) A10. These data demonstrate that functional hemostatic properties determined by ROTEM in $VWF^{RGES/RGES}$ whole blood are comparable to $VWF^{+/+}$ and $VWF^{RGES/+}$ littermates.

Supplemental Figure 5

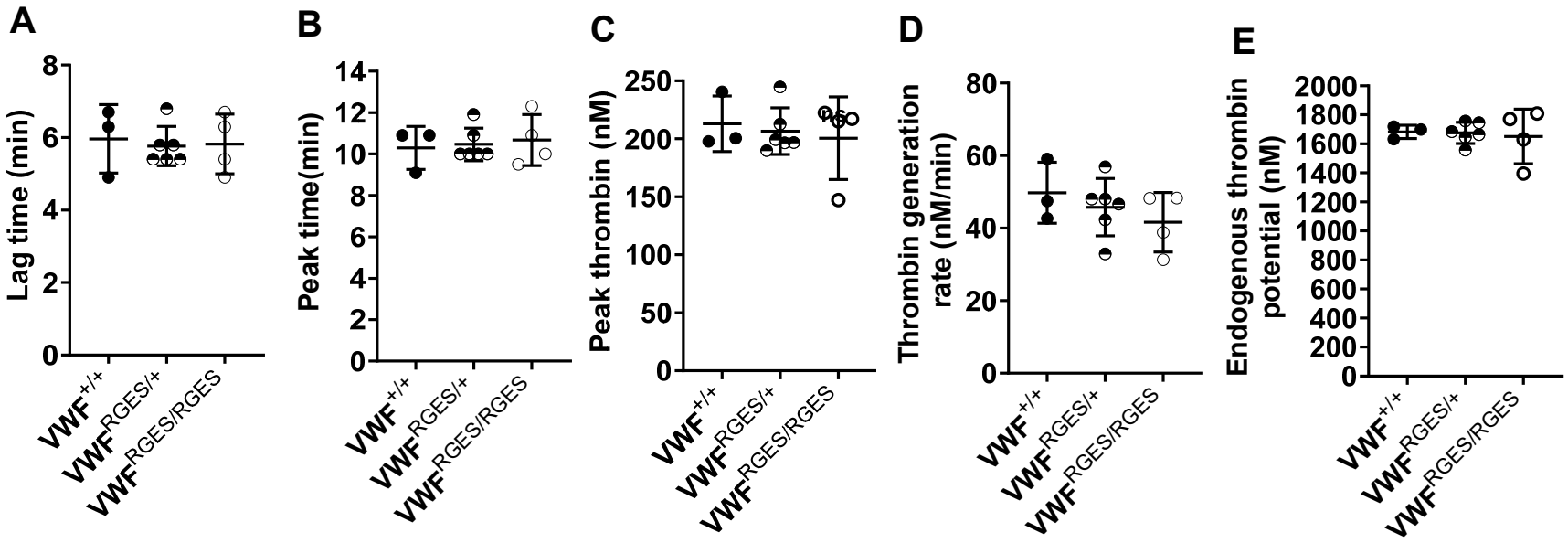

Supplemental Figure 5. Assessment of the biological hemostatic properties in VWF-RGES mice whole blood. Blood samples were collected from the vena cava (terminal experiment) using 3.8% sodium citrate as an anticoagulant (vol/vol 1:10) and analyzed by native whole blood thrombin generation assay (nWB-TGA). Fifteen microliters of whole blood was re-calcified in the presence of a rhodamine-based, thrombin-cleavable, fluorescent substrate and added in duplicate to filter paper placed within the wells of a black 96-well plate. Change in fluorescence was measured over time and converted to thrombin generation. Conversions were calculated from a curve generated during a calibration experiment using a thrombin standard. $VWF^{+/+}$ and $VWF^{RGES/+}$ mice served as controls. (**A**) Lag time. (**B**) Peak time. (**C**) Peak thrombin. (**D**) Thrombin generation rate. (**E**) Endogenous thrombin potential. These data demonstrate that functional hemostatic properties determined by nWB-TGA in $VWF^{RGES/RGES}$ whole blood are comparable to $VWF^{+/+}$ and $VWF^{RGES/+}$ littermates.

Supplemental Figure 6

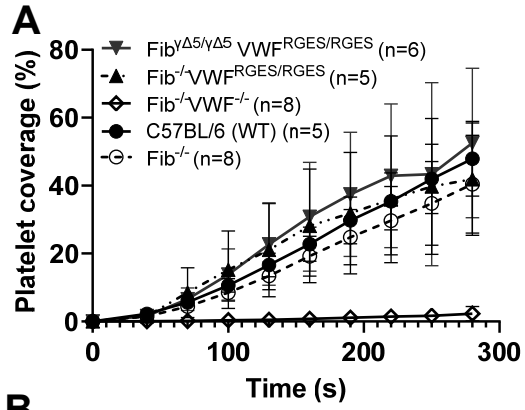

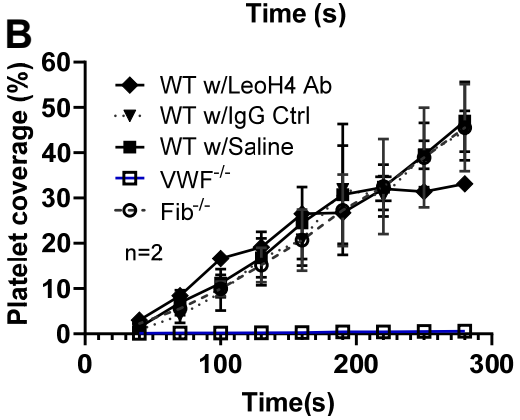

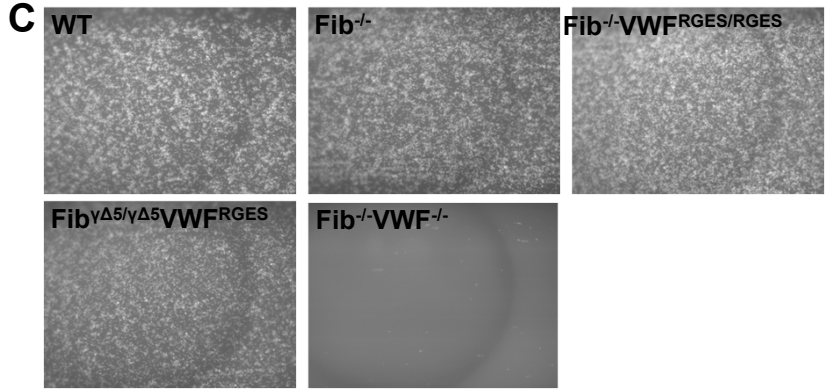

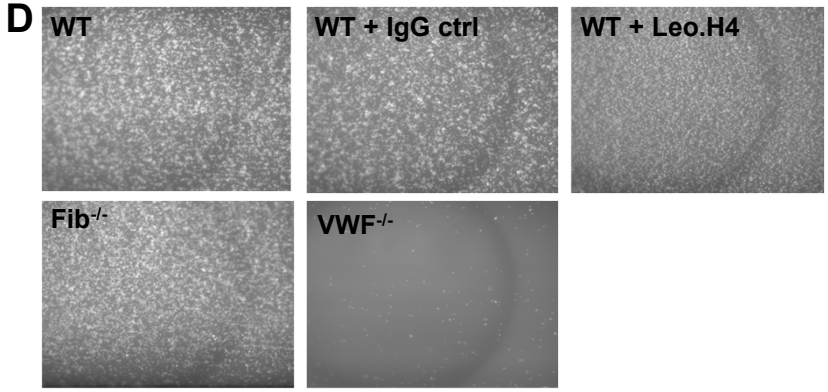

Supplemental Figure 6. Assessment of the impact of VWF-RGES variant on platelet adhesion to collagen from mice whole blood using the VenaFlux microfluidic platform. Blood samples were collected from the vena cava (terminal experiment) using 3.8% sodium citrate as an anticoagulant and 20 μg/ml quinacrine dihydrochloride to stain platelets and infused into a Venaflux chip coated with collagen III under a shear rate of 67.5 dyn/cm. Images were analyzed at the end of the study period. Platelet adhesion was measured by counting the number of platelet aggregates per image (at ×10 original magnification). (**A**) The percentage of platelet coverage on the collagen-coated chip from $Fib^{\gamma\Delta5/\gamma\Delta5}VWF^{RGES/RGES}$ and $Fib^{-/-}VWF^{RGES/RGES}$ mice. $Fib^{-/-}VWF^{-/-}$, $Fib^{-/-}$, and C57BL/6 wild-type (WT) mice were used as controls. (**B**) The percentage of platelet coverage on the collagen-coated chip from WT mouse whole blood treated with anti-GPIIb/IIIa antibody, Leo.H4, which is known to block binding to fibrinogen. WT with IgG or saline, $Fib^{-/-}$, and $VWF^{-/-}$ were used as controls. (**C-D**) Representative images. These data demonstrate that platelets from mice with the VWF-RGES variant can still effectively adhere to collagen as assessed by Venaflux.